18th AIAA/CEAS Aeroacoustics Conference (33rd AIAA Aeroacoustics Conference)
04 - 06 June 2012, Colorado Springs, CO

AIAA 2012-2263

Rotor Inflow Noise Caused by a Boundary Layer: Theory and Examples

Stewart A. L. Glegg[1]
Florida Atlantic University, Boca Raton FL 33431

Michael Morton[2], William Devenport[3]
Virginia Tech, Blacksburg VA 24061

A theory for the noise generated by unsteady loading of an open rotor operating in a turbulent flow is presented. The theory makes no assumptions about the isotropy or homogeneity of the turbulence, and thus can be applied to complex problems such as ingestion of a plane boundary layer into an fan face. The results are illustrated with sample noise calculations for rotors completely and partially immersed in turbulence. When completely immersed the sound spectrum is highly dependent on the advance ratio. For high advance ratios the spectrum has a single broad peak centered slightly above the blade passage frequency. For low advance ratios several peaks (or "haystacks") appear centered on multiples of the blade rate. When partially immersed this multiple-peaked form is greatly enhanced by the modulation of the mean turbulence flow seen by the blades and dominates the spectrum even at low advance ratios.

I. Introduction

Prediction of the noise radiation from fans and propellers usually assumes a uniform inflow. However this rarely happens in practice and in some cases the inflow can be highly distorted. For example the inflow into an embedded engine in an aircraft wing or fuselage is strongly dependent on the characteristics of the mean flow over the body of the aircraft. Another application is wind turbines which operate in the atmospheric boundary layer where the mean flow varies significantly with height above the ground (Oerlemans et al (2007)). The distortion of the inflow can have a significant effect on the radiated noise. For example Hanson (1974) showed how the fan tone noise from an aircraft engine on a test stand was strongly affected by elongated turbulent eddies which were stretched in the axial direction as they were accelerated through the engine intake. Similarly measurements by Sevik (1974) of the unsteady thrust on a 10 bladed propeller showed haystacking about the bade passage tones, which was attributed to anisotropic turbulent eddies entering the rotor (Blake (1986)). This type of turbulence distortion is strongly affected by mean flow shear which is an important component of most real flows.

The distortion of turbulence as it approaches a wind turbine was considered by Amiet et al. (1990). They showed that initially isotropic turbulence becomes significantly anisotropic as a result of the slowing of the mean flow as it approaches the rotor. This effect was considered analytically by Majumder and Peake (1998) who used rapid distortion theory and a potential mean flow to compute the distortion of the turbulence through the engine inlet and also the fan noise which was generated when it interacted with the fan.

In this paper we will describe the background to a propeller noise prediction method that allows for inhomogeneous stretched anisotropic turbulent inflows, such as are found when a propeller is partially embedded in a turbulent boundary layer. We will show how haystacking (broad peaks in the far field spectrum at blade passing frequencies) occurs and give examples on how the rotor size relative to the boundary thickness can cause

1 Professor, Department of Ocean and Mechanical Engineering, AIAA Associate Fellow.

2 Graduate Research Assistant, Department of Aerospace and Ocean Engineering, AIAA Student Member.

3 Professor, Department of Aerospace and Ocean Engineering, AIAA Associate Fellow.

this effect. We will also go onto show how the measurements of the space time correlation functions in a turbulent boundary layer (see companion paper by Morton, Devenport and Glegg(2012)) can be used to predict the far field rotor noise.

Sound radiation from high speed propellers has been studied extensively with comprehensive studies by Farrassat(1986), Hanson(1983), Crighton and Parry(1992), and Peake and Crighton (1992)(see a more comprehensive review in a companion paper by Morton, Devenport and Glegg(2012)). These studies have focused on tone noise and much less work has been done on broadband noise which is the focus of this paper. The classic studies by Sevik(1970) and Ffowcs Williams and Hawkings(1969) demonstrated the basic principles of broadband propeller noise for isotopic turbulence inflows and recent studies by Ataasi and Longue(2009) consider anisotropic flows. In this study we will lay out a comprehensive approach to broadband propeller noise prediction that applies for observers in both the near and far field and allows for arbitrary inflow turbulence modeling. We will assume that the propeller noise problem is characterized by a rotor speed that is relatively fast, so the pure tones developed at blade passing frequencies are well resolved by typical spectral analysis, as distinct from helicopter rotor noise, or the wind turbine noise where the rotor speed is relatively slow and the blade passing tones are not necessarily well resolved unless a very narrow band analysis (<20Hz) is used. On this basis the propeller noise may be considered as stationary in time and the chopping of a large scale eddy by multiple blades will be a key feature of the results. In contrast for the wide bandwidth case the blades will not necessarily re enter the same eddy during the averaging time of the measurement.

Section 2 of this paper presents the basic theory of propeller noise, and section 3 discusses the associated propagation function. In section 4 the modeling of the blade loads is described and then in section 5 the modeling of turbulence in a homogeneous and inhomogeneous flow is specified. Section 6 gives numerical results for a propeller partially submerged in a turbulent flow. The results of this paper are used in a companion paper by Morton, Devenport and Glegg (2012).

2. Sound Radiation from a Propeller

In this section we will give the theory for the sound radiation from an open rotor caused by the unsteady loading on the blades. We start with the solution to Lighthill's wave equation given by Ffowcs Williams and Hawkings(1969) which gives the acoustic field from a blade in arbitrary motion with a net blade surface loading of $f_i(\mathbf{z},\tau)$ per unit area as

$$p'(\mathbf{x},t) = -\frac{\partial}{\partial x_i}\sum_{n=1}^{B}\int_{\Sigma_n}\left[\frac{f_i(\mathbf{z},\tau)}{4\pi r\,|1-M_r|}\right]_{\tau=\tau^*} d\Sigma(\mathbf{z}) \tag{1}$$

In this equation Σ_n represents the surface of each blade and r is the distance from the source point to the observer. The terms in [] are evaluated at the correct retarded time $\tau=\tau^*=t-r/c_o$ and M_r is the Mach number of the source velocity in the direction of the observer. The coordinate system for the analysis is shown in figure 1.

For broadband noise we are interested in calculating the power spectrum of the acoustic field defined as

$$S_{pp}(\mathbf{x},\omega) = \frac{\pi}{T}Ex\left[|\,\hat{p}(\mathbf{x},\omega)\,|^2\right] \qquad \hat{p}(\mathbf{x},\omega) = \frac{1}{2\pi}\int_{-T}^{T} p'(\mathbf{x},t)e^{i\omega t}dt \tag{2}$$

where $\hat{p}(\mathbf{x},\omega)$ is the Fourier transform of the acoustic time signature. We will assume that the time scale $2T$ is large compared to the time taken for one revolution of the rotor so that $\Omega T>>1$. This will ensure that the blade passage tones are fully resolved and that the analysis allows for multiple blade passages through the same turbulent structures.

We can evaluate the Fourier transform in (2) to define the far field spectrum in terms of the source terms by using equation (1). The integral over observer time in (2) can be changed to an integral over emission time because the time differentials are related by $dt=|1-M_r|d\tau$. Since $t=\tau+r(\tau)/c_o$ it follows that

(3)

$$\hat{p}(\mathbf{x},\omega) = -\frac{1}{2\pi}\sum_{n=1}^{B}\frac{\partial}{\partial x_i}\int_{\Sigma_n}\int_{-T}^{T}\frac{f_i(\mathbf{z},\tau)}{4\pi r(\tau)}e^{i\omega(\tau+r(\tau)/c_o)}d\tau d\Sigma(\mathbf{z})$$

We now apply thin airfoil theory so the surface pressure on the upper and lower surfaces of the blade can be combined into a pressure jump $f^{(n)}$ in the lift direction and a drag force per unit area $D^{(n)}$ in the local flow direction. It has been shown by Howe (1989), and Glegg and Devenport(2009) that the drag associated with unsteady loading for an airfoil encountering a gust only occurs when the mean flow is at an angle of attack α to the blade, and is equal to -tan(2α) of the lift force. For small angles of attack it is therefore a reasonable assumption to ignore the drag forces and we will only retain the lift force in the rest of the analysis. The lift force is directed at an angle normal to the inflow angle β (see figure 1) and so can be specified as

(4)

$$f_i(\mathbf{z},\tau) = n_i^{(n)}(R,\tau)f^{(n)}(R,\gamma,\tau) \qquad n_i^{(n)} = (\cos\beta, \sin\beta\sin(\Omega\tau+\phi_n), -\sin\beta\cos(\Omega\tau+\phi_n))$$

where R is the radius and γ is the distance along the blade chord as shown in figure 1, and $\gamma_{LE}<\gamma<\gamma_{TE}$ where γ_{LE},γ_{TE} specifies the leading and trailing edge locations. The axis of the n^{th} blade is located at $\phi=\Omega\tau+\phi_n$ as a function of source time where $\phi_n=2\pi n/B$, as shown in Figure 1 for a rotor that has a angular velocity Ω and an axial speed of V in the x_1 direction. The blade planform is displaced from the axis by ξ as shown in figure 1, and ξ may be a function of radius.

The location of each blade element in the fixed frame of reference is given by

(5)

$$\mathbf{y} = (V\tau - \gamma\sin\beta - \xi\cos\beta, R\cos(\Omega\tau+\phi_n-\phi_b), R\sin(\Omega\tau+\phi_n-\phi_b))$$

where $\phi_b=(\gamma\cos\beta-\xi\sin\beta)/R$. The source position is non periodic because the rotor moves relative to the observer. However in near field or wind tunnel applications we are interested in an observer location that moves at the same speed at the rotor hub in the axial direction. For the moving observer that is at an angle θ_o to the axial direction in hub based coordinates,

(6)

$$\mathbf{x} = (r_o\cos\theta_o + Vt, r_o\sin\theta_o\cos\phi_o, r_o\sin\theta_o\sin\phi_o)$$

The propagation distance r is then given by the solution to the equation

(7)

$$r(\tau) = ((r_o\cos\theta_o + \gamma\sin\beta + \xi\cos\beta + Vr(\tau)/c_o)^2 + (r_o\sin\theta_o\cos\phi_o - R\cos(\Omega\tau+\phi_n-\phi_b))^2 + (r_o\sin\theta_o\sin\phi_o - R\sin(\Omega\tau+\phi_n-\phi_b))^2)^{1/2}$$

It follows that $r(\tau)$ is a periodic function of the source time τ and repeats every blade revolution.

Using these result in (3) gives

(8)

$$\hat{p}(\mathbf{x},\omega) = -\frac{1}{2\pi}\sum_{n=1}^{B}\int_{R_{hub}}^{R_{tip}}\int_{\gamma_{LE}}^{\gamma_{TE}}\int_{-T}^{T}\left\{\frac{\partial}{\partial x_i}\left(\frac{n_i^{(n)}e^{i\omega r(\tau)/c_o}}{4\pi r(\tau)}\right)\right\}f^{(n)}(R,\gamma,\tau)e^{i\omega\tau}d\tau dR d\gamma$$

The functions in {} are periodic in source time and may be expanded in the Fourier series

(9)

$$\left\{\frac{\partial}{\partial x_i}\left(\frac{n_i^{(n)} e^{i\omega r(\tau)/c_o}}{4\pi r(\tau)}\right)\right\} = \frac{i\omega}{c_o r_o}\sum_{m=-\infty}^{\infty} K_{m,n}(R,\gamma,\mathbf{x}) e^{-im(\Omega\tau+\phi_n)}$$

and the evaluation of the integral over source time in equation (8) gives

(10)

$$\hat{p}(\mathbf{x},\omega) = \frac{-i\omega}{c_o r_o}\sum_{n=1}^{B}\sum_{m=-\infty}^{\infty}\int_{R_{hub}}^{R_{tip}}\int_{\gamma_{LE}}^{\gamma_{TE}} K_{m,n}(R,\gamma,\mathbf{x})\hat{f}^{(n)}(R,\gamma,\omega-m\Omega)e^{-im\phi_n} dR d\gamma$$

This result applies to both low and high frequencies and for both the near field and the far field of the rotor. The Fourier coefficients can be evaluated in terms of Bessel and Hankel functions(Hanson (1983)) but can also be calculated by direct numerical evaluation of equation (9). When the blade chord is acoustically compact the dependence of $K_{m,n}$ on both γ and n can be relaxed. In this approximation $\omega\gamma/c_o<<1$ for $\gamma_{LE}<\gamma<\gamma_{TE}$ and the dependence of $r(\tau)$ on γ can be dropped from equation (9), so it is only a function of $\Omega\tau+\phi_n$. The integral over γ in (10) then yields the unsteady lift on the blade section so

(11)

$$\hat{p}(\mathbf{x},\omega) = \frac{-i\omega}{c_o r_o}\sum_{n=1}^{B}\sum_{m=-\infty}^{\infty}\int_{R_{hub}}^{R_{tip}} K_m(R,\mathbf{x})L^{(n)}(R,\omega-m\Omega)e^{-im\phi_n} dR$$

where

(12)

$$L^{(n)}(R,\omega) = \int_{\gamma_{LE}}^{\gamma_{TE}} \hat{f}^{(n)}(R,\gamma,\omega) d\gamma$$

In order to calculate the spectrum of the radiated sound we need to specify the spectrum of the unsteady loads. If the averaging time is large enough ($\Omega T>>1$) then the unsteady loading spectrum will be uncorrelated at different frequencies, and we obtain

(13)

$$S_{pp}(\mathbf{x},\omega) =$$
$$\left(\frac{\omega}{c_o r_o}\right)^2 \sum_{n=1}^{B}\sum_{k=1}^{B}\sum_{m=-\infty}^{\infty}\int_{R_{hub}}^{R_{tip}}\int_{R_{hub}}^{R_{tip}} K_m(R,\mathbf{x})K_m^*(R',\mathbf{x})S_{LL}^{(n,k)}(R,R',\omega-m\Omega)e^{-im(\phi_n-\phi_k)} dR dR'$$

where

(14)

$$S_{LL}^{(n,k)}(R,R',\omega) = \frac{\pi}{T} Ex[L^{(n)}(R,\omega)L^{(k)}(R',\omega)^*]$$

is the power spectrum of the unsteady blade loads.

This equation is the basis of the broadband propeller noise theory described in this paper. It strictly only applies to propellers with compact chords, but can be extended to higher frequency applications without much difficulty. It applies in both the near and far fields for wind tunnel coordinates, but can also be extended to a fixed far field observer and a moving propeller. A similar expression can be obtained from Hanson's (1983) helicoidal surface theory for propeller noise.

3. Far Field Approximations

For an observer in the acoustic far field the expansion given by (9) can be evaluated directly. Using the approximation $r \sim |\mathbf{x}| - \mathbf{x}.\mathbf{y}/|\mathbf{x}|$ and assuming that blade chord is compact, it follows, that for the blade element at radius R and azimuthal location $\Omega\tau+\phi_n$ (see Figure 1), the propagation distance can be approximated as

(15)

$$r(\tau) \approx r_o - R\sin\theta_o \cos(\phi_n - \phi_o + \Omega\tau)$$

We then make use of the Fourier series expansion

(16)

$$e^{-i\alpha\cos\theta} = \sum_{m=-\infty}^{\infty} J_m(\alpha) e^{-im(\theta+\pi/2)}$$

where $J_m(\alpha)$ is a Bessel function of the first kind of order m, so

(16)

$$e^{i\omega r(\tau)/c_o} = e^{i\omega r_o/c_o} \sum_{m=-\infty}^{\infty} J_m\left(\frac{\omega R\sin\theta_o}{c_o}\right) e^{-im(\phi-\phi_o+\Omega\tau+\pi/2)}$$

Combining these results gives and assuming that $\beta << 1$ then gives

(17)

$$K_m(R,\mathbf{x}) = \frac{\cos\theta_o}{4\pi} J_m\left(\frac{\omega R\sin\theta_o}{c_o}\right) e^{i\omega r_o + im(\phi_o-\pi/2)}$$

4. The Unsteady Load Spectrum

For thin blades the unsteady loading can be calculated by assuming they can be modeled as a flat plate at zero angle of attack. The effect of loading is to alter the direction of the loading force, but not it's amplitude, and is ignored for small angles of attack as described above. The effect of blade thickness tends to reduce the high frequency response of the rotor, but will not be included here. The effect of blade camber is small providing the angle of attack is taken to be the entry angle to the blade (see Glegg and Devenport(2010)). Given these assumptions we can specify the unsteady blade loading to be proportional to the upwash velocity encountered by the blade as specified by Sears(1949), who considered the response of a flat plate to a harmonic upwash gust specified as $w_o exp(-ik(U_e t - x))$. Sears gives

(18)

$$L_o(\tau) = \pi\rho_o c U_e w_o S(\sigma) e^{-i\omega\tau} \qquad \sigma = \omega c / 2U_e \qquad S = \frac{2}{\pi\sigma(H_0^{(1)}(\sigma) + iH_1^{(1)}(\sigma))}$$

For a more general gust which is swept by the airfoil at the mean convection speed of the local blade section U_e, the blade response can be calculated from the Fourier transform with respect to time of the upwash velocity at the leading edge of the blade, specified as $w^{(n)}(\omega,R)$. This gives the unsteady lift spectrum as

(19)

$$L^{(n)}(\omega,R) = \pi\rho_o c U_e S(\sigma(R)) w^{(n)}(R,\omega)$$

Using these results, the unsteady loading spectrum caused by turbulence ingestion can be defined as

(20)

$$S_{LL}^{(n,k)}(\omega,R,R') = \left[\pi\rho_o c U_e S(\sigma)\right]_{R=R} \left[\pi\rho_o c U_e S(\sigma)\right]^*_{R=R'} S_{ww}^{(n,k)}(\omega,R,R')$$

$$S_{ww}^{(n,k)}(\omega,R,R') = \left\{\frac{\pi}{T} Ex[w^{(n)}(R,\omega) w^{(k)}(R',\omega)^*]\right\}$$

If we define $\mathbf{z}^{(n)}(\tau)$ as the location in hub fixed coordinates of the n^{th} blade at source time τ, and the flow velocity in the rotor plane relative to the hub as $U_{hub}\hat{\mathbf{x}} + \Delta\mathbf{U}(\mathbf{y}) + \mathbf{v}(\mathbf{y},t)$ where $\Delta\mathbf{U}$ is the variation of the mean velocity in the rotor disc plane relative to the mean flow velocity at the rotor hub, and $\mathbf{v}$ is the turbulent flow velocity, then the upwash velocity caused by turbulence is

(21)

$$w^{(n)}(R,\omega) = \frac{1}{2\pi}\int_{-T}^{T} n_i^{(n)}(R,\tau) v_i(\mathbf{z}_n(\tau),\tau) e^{i\omega\tau} d\tau$$

where $n_i^{(n)}$ is the blade surface normal to the n^{th} blade as defined in equation (4). Utilizing this result we obtain

(22)

$$S_{ww}^{(n,k)}(\omega,R,R') = \frac{1}{4\pi^2}\frac{\pi}{T}\int_{-T}^{T}\int_{-T}^{T} n_i^{(n)}(R,\tau) n_j^{(k)}(R',\tau') R_{ij}(\mathbf{z}_n(\tau),\mathbf{z}_k(\tau'),\tau-\tau') e^{i\omega(\tau-\tau')} d\tau d\tau'$$

where $R_{ij}(\mathbf{x},\mathbf{y},t)$ is the cross correlation function of the turbulent velocity in the plane of the rotor. This is the quantity which needs to be evaluated for turbulence ingestion noise and is the focus of this study.

5. Turbulence Ingestion Noise in a Homogeneous and Inhomogeneous Flow

To understand the important features of the upwash spectrum it is valuable to consider the idealized case in which the inflow turbulence is homogeneous. The cross correlation of the turbulent stresses can then be modeled as

(23)

$$R_{ij}(\mathbf{x},\mathbf{y},t) = \int_{\mathbf{k}} \Phi_{ij}(\mathbf{k}) e^{-i\mathbf{k}.(\mathbf{x}-\mathbf{y}-\mathbf{U}_{hub}t)} d\mathbf{k}$$

and so

(24)

$$S_{ww}^{(n,k)}(\omega,R,R') = \frac{1}{4\pi^2}\int_{\mathbf{k}} \Phi_{ij}(\mathbf{k}) \frac{\pi}{T}\int_{-T}^{T}\int_{-T}^{T} n_i^{(n)}(R,\tau) n_j^{(k)}(R',\tau') e^{-i\mathbf{k}.(\mathbf{z}_n(\tau)-\mathbf{z}_k(\tau'))+i(\omega+\mathbf{k}.\mathbf{U}_{hub})(\tau-\tau')} d\tau d\tau' d\mathbf{k}$$

This expression is greatly simplified if we recognize the periodicity of the terms and define

(25)

$$n_i^{(n)}(R,\tau)e^{-i\mathbf{k}.\mathbf{z}_n(\tau)} = \sum_{s=-\infty}^{\infty} Z_{s,i}^{(n)}(R)e^{-is\Omega\tau}$$

so

$$S_{ww}^{(n,k)}(\omega,R,R') = \frac{1}{4\pi^2}\int_{\mathbf{k}} \Phi_{ij}(\mathbf{k})\sum_{s=-\infty}^{\infty}\sum_{t=-\infty}^{\infty} Z_{s,i}^{(n)}(R)Z_{t,j}^{(k)}(R')\frac{\pi}{T}\int_{-T}^{T}\int_{-T}^{T} e^{-is\Omega\tau+it\Omega\tau'+i(\omega+\mathbf{k}.\mathbf{U}_{hub})(\tau-\tau')}d\tau d\tau' d\mathbf{k}$$

We then evaluate the integral as

$$\frac{\pi}{T}\int_{-T}^{T}\int_{-T}^{T} e^{-is\Omega\tau+it\Omega\tau'+i(\omega+\mathbf{k}.\mathbf{U}_{hub})(\tau-\tau')}d\tau d\tau' = (2\pi)^2\delta(s\Omega-\omega-\mathbf{k}.\mathbf{U}_{hub})\frac{\sin((t\Omega-\omega-\mathbf{k}.\mathbf{U}_{hub})T)}{(t\Omega-\omega-\mathbf{k}.\mathbf{U}_{hub})T}$$

which is only non zero when $s=t$ and yields

(26)

$$S_{ww}^{(n,k)}(\omega,R,R') = \sum_{s=-\infty}^{\infty}\int_{\mathbf{k}} Z_{s,i}^{(n)}(R)Z_{s,j}^{(k)}(R')\Phi_{ij}(\mathbf{k})\delta(s\Omega-\omega-\mathbf{k}.\mathbf{U}_{hub})d\mathbf{k}$$

Note that broadband noise only occurs when the axial flow velocity is non zero. If this were not the case then the flow pattern experienced by the rotor would be the same on every revolution and the radiated noise would only occur at the blade passage frequencies. The axial flow speed of the turbulence is therefore important and the characteristics of this result are best illustrated by considering a simple example.

Example 1: A fan with untwisted blades

A fan with untwisted blades is a simple example of a propeller in which the blade chord and inflow angle are constant at each blade section. We can also assume that the inflow angle is small so $\beta<<1$. Given this approximation $n_i^{(n)}=(1,0,0)$ and

(27)

$$\mathbf{z}^{(n)}(\tau) = (0, R\cos(\phi_n+\Omega\tau), R\sin(\phi_n+\Omega\tau))$$

It follows that

(28)

$$n_1^{(n)}(R,\tau)e^{-i\mathbf{k}.\mathbf{z}_n(\tau)} = e^{-ik_R R\cos(\phi_n+\Omega\tau-\kappa)} = \sum_{s=-\infty}^{\infty} i^s J_s(k_R R)e^{-is(\Omega\tau+\phi_n-\kappa)}$$

so

$$S_{ww}^{(n,k)}(\omega,R,R') = \sum_{s=-\infty}^{\infty}\int_{-\infty}^{\infty}\int_{0}^{\infty}\int_{0}^{2\pi}\Phi_{11}(\mathbf{k})J_s(k_R R)J_s(k_R R')e^{-is(\phi_n-\phi_k)}\delta(s\Omega-\omega-k_1U_{hub})dk_1k_R dk_R d\kappa$$

where $k_R^2=k_2^2+k_3^2$ and $\kappa=\tan^{-1}(k_3/k_2)$.

To model the turbulence we will assume that it is anisotropic and use the Gleibe Kerschen model to give

(29)

$$\Phi_{11}(k_1,k_R)=\frac{2L_t^2L_au_a^2(k_RL_t)^2}{\pi^2(1+(k_RL_t)^2+(k_1L_a)^2)^6}$$

where L_a is the axial lengthscale, L_t is the transverse lengthscale, and u_a is the axial turbulence intensity. Hence

(30)

$$S_{ww}^{(n,k)}(\omega,R,R')=\frac{4L_au_a^2}{\pi U_{hub}}\sum_{s=-\infty}^{\infty}\int_0^{\infty}\frac{(k_RL_t)^3J_s(k_RR)J_s(k_RR')e^{-is(\phi_n-\phi_k)}}{(1+((s\Omega-\omega)L_a/U_{hub})^2+(k_RL_t)^2)^6}d(k_RL_t)$$

This result indicates that the upwash turbulence spectra will have broad peaks at the shaft rotation frequencies where $\omega=s\Omega$ and the width of the peaks will scale on $\omega L_a/U_{hub}$. We also note that when $\Omega L_a/U_{hub}>>1$ then the peaks are distinct, but when $\Omega L_a/U_{hub}\sim 1$ then the peaks merge and a broadband spectrum is obtained.

The acoustic field from the fan can be obtained from equation (13) above as

(31)

$$S_{pp}(\mathbf{x},\omega)=\left(\frac{\omega\cos\theta_o}{4\pi r_oc_o}\right)^2$$
$$\times\sum_{n=1}^{B}\sum_{k=1}^{B}\sum_{m=-\infty}^{\infty}\int_{R_{hub}}^{R_{tip}}\int_{R_{hub}}^{R_{tip}}J_m\left(\frac{\omega R\sin\theta_o}{c_o}\right)J_m\left(\frac{\omega R'\sin\theta_o}{c_o}\right)S_{LL}^{(n,k)}(R,R',\omega-m\Omega)e^{im(\phi_n-\phi_k)}dRdR'$$

where we have used equation (18). Combining results and separating terms gives

(32)

$$S_{pp}(\mathbf{x},\omega)=\left(\frac{\omega c\cos\theta_o}{r_oc_o}\right)^2\frac{\rho_o^2L_au_a^2}{4\pi U_{hub}}$$
$$\sum_{n=1}^{B}\sum_{k=1}^{B}e^{-i(m+s)(\phi_n-\phi_k)}\sum_{m=-\infty}^{\infty}\sum_{s=-\infty}^{\infty}\int_0^{\infty}\left|\int_{R_{hub}}^{R_{tip}}J_m\left(\frac{\omega R\sin\theta_o}{c_o}\right)J_s(k_RR)S\left(\frac{(\omega-m\Omega)c}{2U_e(R)}\right)dR\right|^2$$
$$\frac{(k_RL_t)^3}{(1+(((s+m)\Omega-\omega)L_a/U_{hub})^2+(k_RL_t)^2)^6}d(k_RL_t)$$

Noting that $\phi_n=2\pi n/B$ shows that the summations over n and k are only non zero when $s+m=jB$ where j is an integer. Hence this result can be simplified as

(33)

$$S_{pp}(\mathbf{x},\omega)=\left(\frac{\omega c\cos\theta_o}{r_oc_o}\right)^2\frac{\rho_o^2L_au_a^2B^2}{4\pi U_{hub}}\sum_{j=-\infty}^{\infty}\int_0^{\infty}\frac{D_j(\omega,k_R,\theta_o)(k_RL_t)^3}{(1+((jB\Omega-\omega)L_a/U_{hub})^2+(k_RL_t)^2)^6}d(k_RL_t)$$

$$D_j(\omega,k_R,\theta_o)=\sum_{m=-\infty}^{\infty}\left|\int_{R_{hub}}^{R_{tip}}J_m\left(\frac{\omega R\sin\theta_o}{c_o}\right)J_{jB-m}(k_RR)S\left(\frac{(\omega-m\Omega)c}{2U_e(R)}\right)dR\right|^2$$

Although this is a complicated expression it can be evaluated numerically without much difficulty. We note that the peaks in the spectrum should occur at the blade passing frequencies and that the width of the peaks will depend on $\Omega L_a/U_{hub}$. We will illustrate the features of the spectrum with some examples as given below.

Example 2: A fan in inhomogeneous flow

The example given above for a fan with untwisted blades in homogeneous flow can be easily extended to the case of an inhomogeneous flow where the turbulence only wets part of the rotor disc plane. The turbulence is assumed to be zero when $y_2>d$ and the correlation function is modeled as

$$R_{ij}^{(M)}(\mathbf{x},\mathbf{y},\tau) = H(d-y_2)H(d-x_2)R_{ij}(\mathbf{x},\mathbf{y},\tau) \tag{34}$$

where R_{ij} is the correlation function of homogeneous turbulence and the impact of the edges of the turbulence have been ignored, although they may be the dominant effect. Given this idealized model we can modify equation (25) to take account of the inhomogeneity by using

$$H(d-R\cos(\Omega\tau+\phi_n))n_1^{(n)}(R,\tau)e^{-i\mathbf{k}\cdot\mathbf{z}_n(\tau)} = H(d-R\cos(\Omega\tau+\phi_n))e^{-ik_R R\cos(\phi_n+\Omega\tau-\kappa)}$$

$$= \sum_{s=-\infty}^{\infty} Y_s(k_R R,\kappa,d)e^{-is(\Omega\tau+\phi_n)}$$

so

$$S_{ww}^{(n,k)}(\omega,R,R') = \sum_{s=-\infty}^{\infty}\int_{-\infty}^{\infty}\int_{0}^{\infty}\int_{0}^{2\pi}\Phi_{11}(\mathbf{k})Y_s(k_R R,\kappa,d)Y_s(k_R R',\kappa,d)$$
$$\times e^{-is(\phi_n-\phi_k)}\delta(s\Omega-\omega-k_1U_{hub})dk_1dk_Rd\kappa$$

The coefficients Y_s can be calculated from the integral

$$Y_s(k_R R,\kappa,d) = \frac{1}{2\pi}\int_{\varphi_1}^{2\pi-\varphi_1} e^{-ik_R R\cos(\varphi-\kappa)+is\varphi}d\varphi \qquad \varphi_1 = \begin{cases}\pi & d<-R\\ \cos^{-1}(d/R) & |d|<R\\ 0 & d>R\end{cases}$$

giving

$$Y_s(k_R R,\kappa,d) = \frac{1}{2\pi}\int_{\varphi_1}^{2\pi-\varphi_1}\sum_{u=-\infty}^{\infty}J_u(k_R R)e^{i(s-u)\varphi+iu\kappa}d\varphi = \sum_{u=-\infty}^{\infty}J_u(k_R R)e^{iu\kappa}F_{u-s}$$

$$F_{u-s} = \begin{cases}\dfrac{\sin((u-s)\varphi_1)}{(u-s)\pi} & u\neq s\\ 1-\varphi_1/\pi & u=s\end{cases}$$

and we find

$$S_{ww}^{(n,k)}(\omega,R,R') = \sum_{s=-\infty}^{\infty}\sum_{u=-\infty}^{\infty}\sum_{v=-\infty}^{\infty}\int_{-\infty}^{\infty}\int_{0}^{\infty}\int_{0}^{2\pi}\Phi_{11}(\mathbf{k})J_u(k_R R)J_v(k_R R')$$
$$\times F_{u-s}F_{v-s}e^{-is(\phi_n-\phi_k)-i(u-v)\kappa}\delta(s\Omega-\omega-k_1U_{hub})dk_1dk_R d\kappa$$

which on integrating over κ gives

$$S_{ww}^{(n,k)}(\omega,R,R') = 2\pi\sum_{s=-\infty}^{\infty}\sum_{u=-\infty}^{\infty}\int_{-\infty}^{\infty}\int_{0}^{\infty}\Phi_{11}(\mathbf{k})J_u(k_R R)J_u(k_R R')$$
$$\times F_{u-s}^2 e^{-is(\phi_n-\phi_k)}\delta(s\Omega-\omega-k_1U_{hub})dk_1dk_R$$

Then the analysis remains the same as in the previous example only the D_j function is modified to

$$D_j(\omega,k_R) = \sum_{m=-\infty}^{\infty}\sum_{u=-\infty}^{\infty}\left|\int_{R_{hub}}^{R_{tip}} J_m\left(\frac{\omega R\sin\theta_o}{c_o}\right)J_u(k_R R)F_{jB-m-u}S\left(\frac{(\omega-m\Omega)c}{2U_e(R)}\right)dR\right|^2$$

which may be used in (33) to give the radiated sound field.

6. Results and Discussion

The results for the examples given above have been evaluated for the case when the tip Mach number is 0.1 and the axial flow speed has a Mach number of 0.15. The axial lengthscale is taken as twice the transverse lengthscale, and the rotor has four blades. The observer is at 45º to the rotor axis.

The spectrum for the first example is shown in Figure 2 and is seen to have a broad peak close to the blade passing frequency, but the peak is skewed and the peak frequency is slightly higher than blade passing frequency. The spectrum is dominated by the *j=1* term in the series given in equation (33), and also shown in this figure are the contributions of the *j=2* and the *j=3* terms, which peak slightly above the second an third multiple of blade passing frequency.

The reason the peaks are skewed is because the function D_j which is an important weighting factor in equation (33) tends to increase with frequency as shown in Figure 3. This is a consequence of the radiation efficiency of each mode increasing with frequency. In addition the radiated sound has an additional factor of ω^2 associated with the radiation efficiency, and these combined effects cause the broad peaks around blade passage frequency to be skewed, with a weighting towards higher frequencies.

However if the flow speed through the rotor is reduced from a Mach number of 0.15 to a Mach number of 0.05, so that it is less than the tip Mach number, then the spectrum is dominated by symmetrical and distinct peaks at the blade passage, as shown in Figure 4.

Finally we will consider the case when the axial flow Mach number is very much greater than the tip Mach number. Figure 5 shows the case when the axial flow Mach number is 0.5 and the tip Mach number is 0.1. This shows a broad peak and the peak frequency is at $2B\Omega$, inducating clearly that the peak frequency increases with axial flow speed when all other parameters are held constant.

From this we conclude that the advance ratio of the rotor has a large effect on the shape of the far field noise spectrum. If the advance ratio is large $U_a >> \Omega R_{tip}$ then the spectrum is dominated by a broad peak centered slightly above the blade passing frequency. If, on the other hand, the advance ratio is small then the spectrum has multiple peaks which are centered on each multiple of the blade passing frequency. It

should be noted that we have only considered turbulence noise in this study and the noise from the mean flow distortions which cause blade passage tones must be superimposed on these results.

In the second example we considered the same fan in inhomogeneous turbulence. In this case the rotor was partially immersed in a bounded turbulent flow, and the effect of immersion was modeled. The analysis provided a relatively simple expression to evaluate for the radiate noise and the effect of rotor immersion depth. Figure 6 shows the radiated noise spectrum from a rotor in which the turbulence only extends half way across the radius. For example in a wind turbine application, where the rotor axis is horizontal, the turbulence would extend from the ground to half a radius below the hub. The same turbulence parameters used in Figure 2 are used in the calculations given in Figure 6, but the spectrum shape is dramatically different, with distinct narrow peaks around the blade passing frequencies caused by the modulation of the mean turbulent flow encountered by the blades. It should be noted that there will also be blade passage tones superimposed on this spectrum which are not included in this calculation.

7. Conclusions

This paper presents the background theory and some numerical examples of the broadband noise from a propeller operating in an anisotropic inhomogeneous turbulent flow. The basic theory for the propeller noise is an extension of existing theories of propeller noise to encompass the broadband noise case, and applies for both near field and far field observers. The main contribution of this paper is the specification of the form of the turbulence correlation function required for broadband noise calculations. This needs to include the impact of blade to blade correlation as well as the anisotropy and inhomogeneity of the turbulence. The particular form of this function is described by equation (22) which gives the spectrum of the upwash velocity encountered by the blades. A detailed study of this function is provided in a companion paper by Morton, Devenport and Glegg(2012). This result fully accounts for the multiple chopping of turbulent structures by blades and can be related to measurements of the space time correlation function at the inflow plane of the propeller. Numerical examples are given that show how different parameters affect the spectral shape of the radiated sound. For large advance ratios the spectrum is dominated by a large peak that occurs at a frequency just above the blade passing frequency. For low advance ratio propellers the spectrum has multiple peaks, or haystacks, centered on the blade passing frequency.

Acknowledgements

The authors would like to thank the Office of Naval Research, in particular Drs. Ki-Han Kim and John Muench, under grants N00014-10-1-0908 and N00014-10-1-0910. We would also like to acknowledge Dr. Bill Blake for his helpful suggestions and insight.

References

Amiet, R.K.,Simonich, J.C., and Schlinker, R.H., (1990) Journal of Aircraft 27, pp15-22. “Rotor noise due to atmospheric turbulence ingestion,Part II: aeroacoustic results””

Atassi H.M., and Logue M.M, (2009) “Fan Broadband Noise in Anisotropic Turbulence”, AIAA paper no. 2009-3148

Blake, W., (1986) Mechanics of Flow Induced Sound and Vibration, Wiley, New York, 1986

Crighton D.G. and A.B. Parry, (1992) Higher approximations in the asymptotic theory of propeller noise, AIAA Journal, 30, 23-28.

Farrasat, F., (1986), “prediction of Advanced Propeller Noise in the Time Domain”, AIAA Journal Vol 24, No. 4, pp499-504.

Ffowcs Williams, J.E and Hawkings D.L., “Sound Generation by Turbulence and Surfaces in Arbitrary Motion”, Phil. Trans. Roy. Soc. London, A264, 1969, 321-342.

Ffowcs Williams, J.E and Hawkings D.L., “Sound Generation by Rotating Machinery”, Journal of Sound and Vibration, Vol, 1969.

S. Glegg and W. Devenport, "Unsteady loading on an airfoil of arbitrary thickness", Journal of Sound and Vibration, vol 319, pp. 1252-1270., 2009

Gleibe, P.E., and Kerschen, E.J., (1980), “Analytical study of the effects of wind tunnel turbulence on rotor noise”, NASA CR 152359

Hanson, D. B.(1974) Spectrum of Rotor Noise Caused by Atmospheric Turbulence. J. Acoust. Soc.Am., vol.56,no.1.

Hanson, D., 1983, “Compressible Helicoidal Surface Theory Propeller Aerodynamics and Noise,” AIAA J., 21, pp. 881–889.

Metzger, F., 1995, “A Review of Propeller Noise Prediction Methodology 1919–1994,” NASA Technical Report No. CR-198156.

Morton,.M., Devenport, W., and Glegg, S., 2012, “Rotor inflow noise caused by a boundary layer: Inflow measurements and noise predictions”, AIAA 18th AIAA/CEAS Aeroacoustics Conference, June 4th-6th 2012, Colorado Springs, CO

Oerlemans, S., Sijtsma, P. and Méndez López, B., (2007) J. Sound Vib. Vol 299, Pages 869-883, “Location and quantification of noise sources on a wind turbine”

Peake, N., and Crighton D.G., (1991), “An asymptotic theory of near-field propeller acoustics “, Journal of Fluid Mechanics , 232 : pp 285-301

Robison, RAV and Peake, N (2010) Propeller unsteady distortion noise. 16th AIAA/CEAS Aeroacoustics Conference (31st AIAA Aeroacoustics Conference)

Sevik, M.,(1970) “Sound Radiation from a Subsonic Rotor Subjected to Turbulence,” Symposium on Fluid Mechanics, Acoustics and Design of Turbomachinery, August 31 to September 3, 1970, The Pennsylvania State University, NASA SP 304.

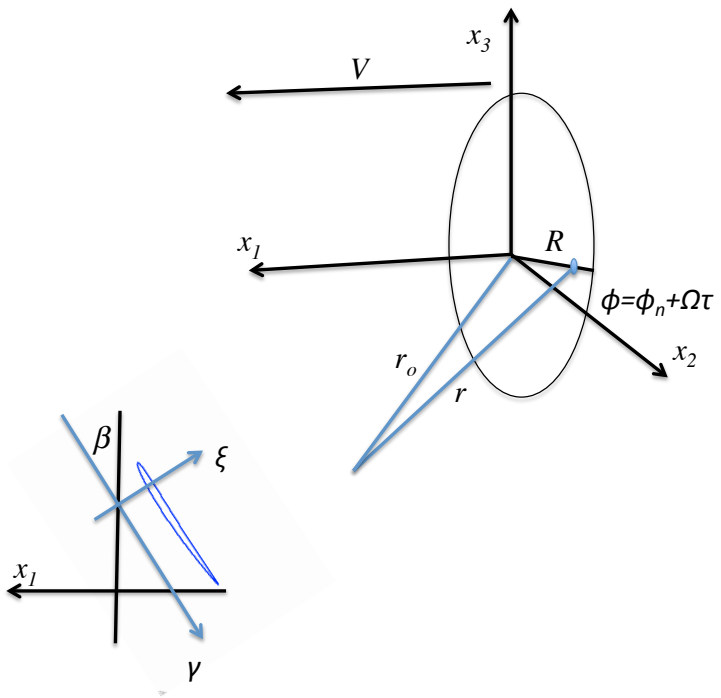

Figure 1: The coordinate system showing the propeller disc plane and the observer location.

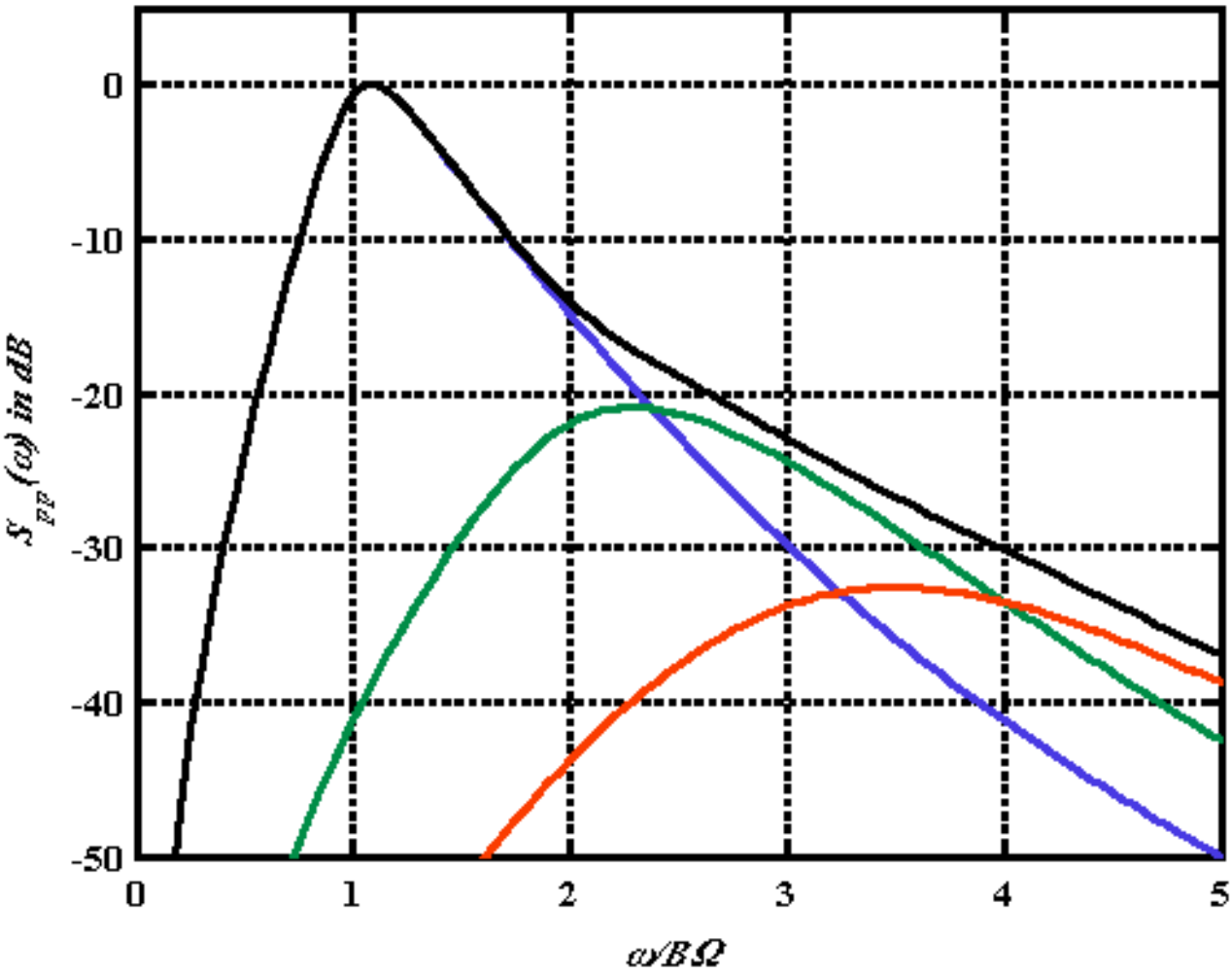

Figure 2: The far field noise spectrum for a flat bladed rotor in homogeneous turbulence U_a=0.15,L_t=1, L_a=2 and M_{tip}=0.1. Curves for total noise (black), *j=1* (blue), *j=2* (green), *j=3* (red)

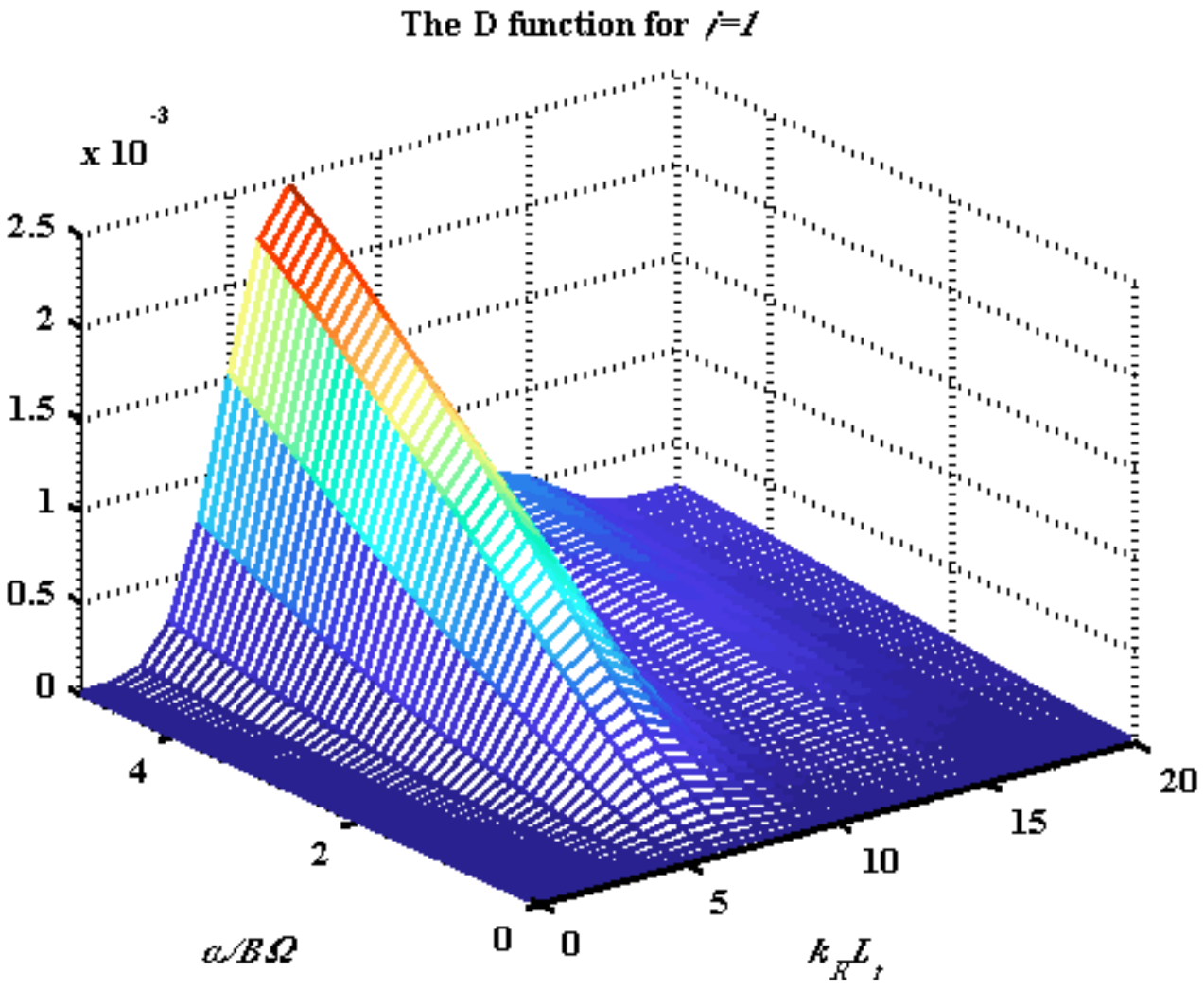

Figure 3: The D function for the blade passing frequency peak for the conditions shown in Figure 2.

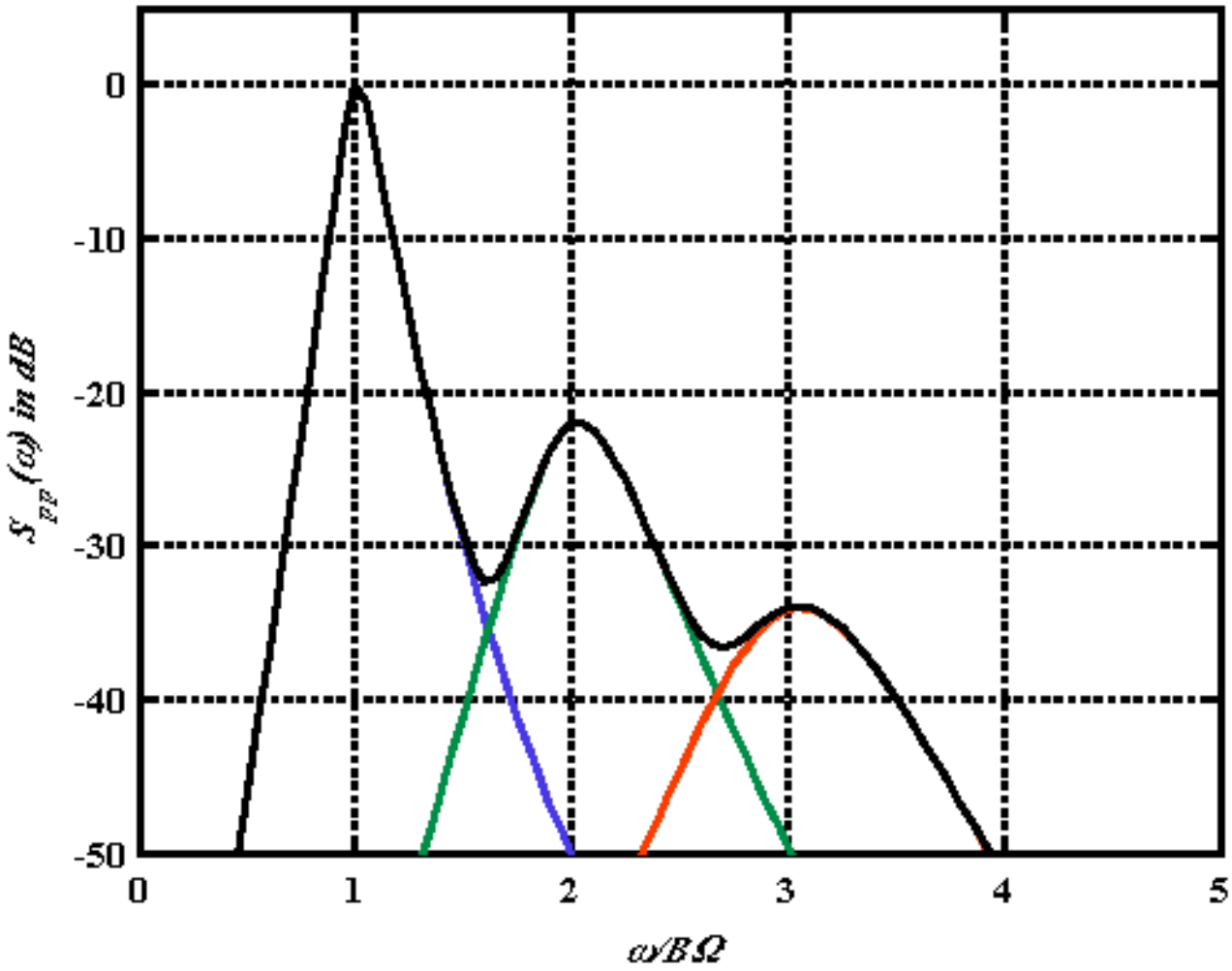

Figure 4: The far field noise spectrum for a flat bladed rotor in homogeneous turbulence $U_a=0.05$, $L_t=1$, $L_a=2$ and $M_{tip}=0.1$. Curves for total noise (black), $j=1$ (blue), $j=2$ (green), $j=3$ (red)

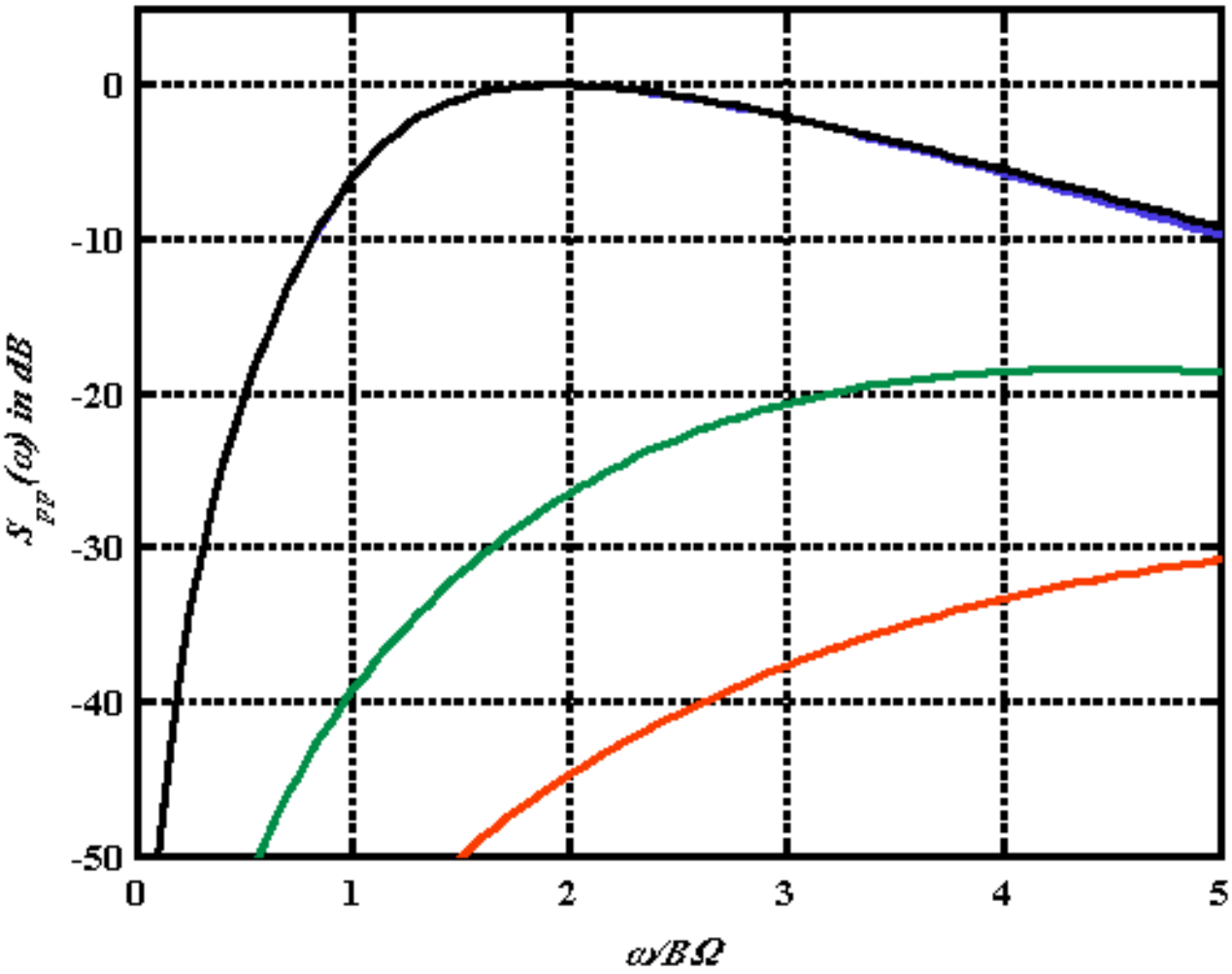

Figure 5: The far field noise spectrum for a flat bladed rotor in homogeneous turbulence U_a=0.5 L_t=1, L_a=2 and M_{tip}=0.1. Curves for total noise (black), *j=1* (blue), *j=2* (green), *j=3* (red)

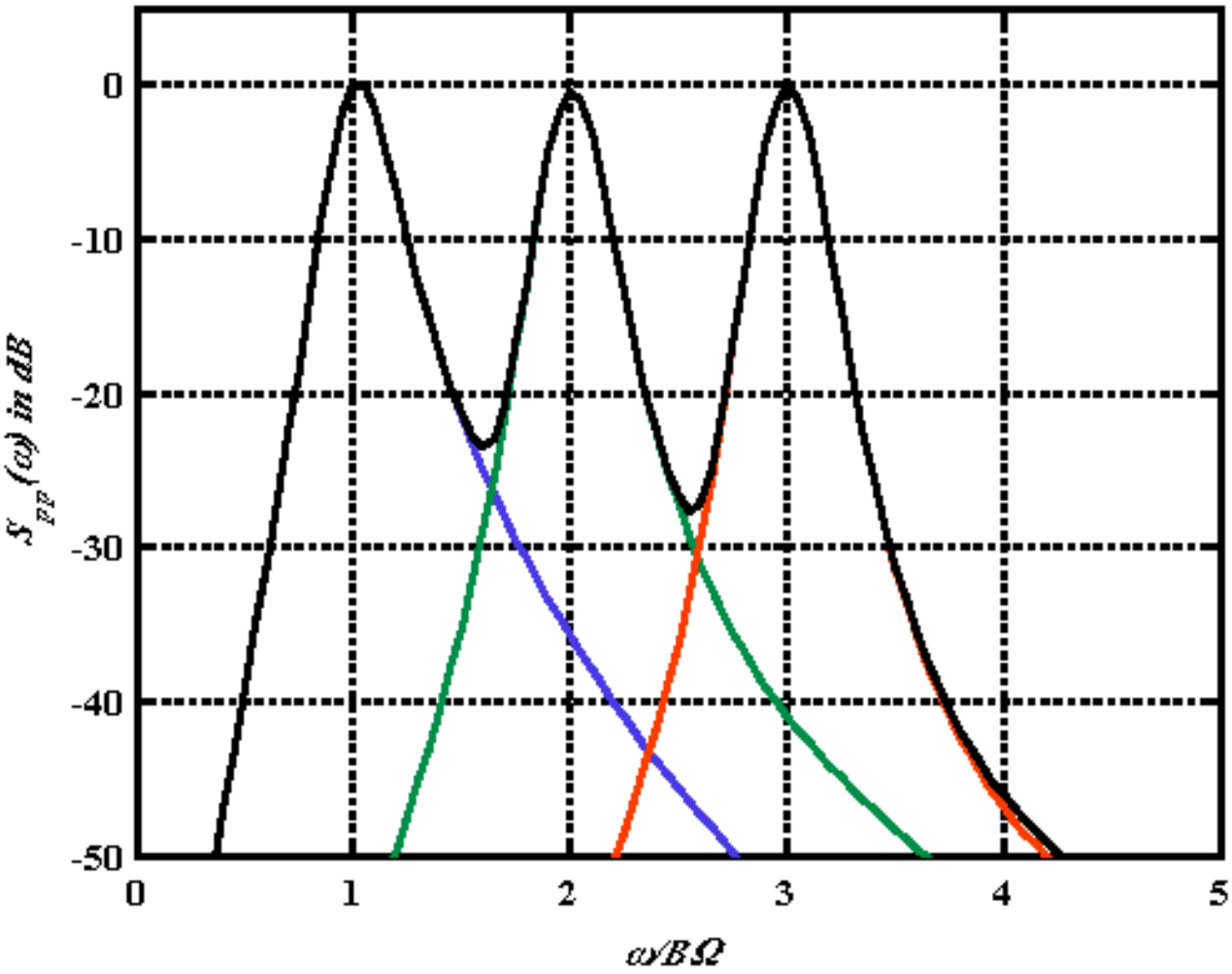

Figure 6: The far field noise spectrum for rotor partially immersed in a turbulent flow, *d=-0.5*, U_a*=0.15*, L_t*=1*, L_a*=2* and M_{tip}*=0.1*. Curves for total noise (black), *j=1* (blue), *j=2* (green), *j=3* (red).